# Dense Delta-Sigma Phased Arrays

James D. Krieger, Chen-Pang Yeang, *Member, IEEE*, and Gregory W. Wornell, *Fellow, IEEE*

***Abstract*—The high cost of high-resolution phase shifters required to maintain precise control over the array beam pattern in traditional phased arrays preclude their use in a variety of emerging millimeter-wave applications. We develop a phased array architecture that obviates the need for such precise phase shifters, based on the use of sub-half-wavelength array element spacing and novel spatial domain delta-sigma processing. We characterize the performance of this architecture in terms of the array signal-to-quantization-noise ratio (SQNR) and the array power transfer efficiency, and demonstrate a tradeoff between these two metrics. As an illustrative design, we show that when constrained to two-bit phase shifters, a four-fold increase in the array density can provide a roughly 6 dB improvement in SQNR over standard design techniques, with an average efficiency loss of less than 1.5 dB with respect to a perfectly tuned ideal array. In our analysis, we account for the effects of mutual coupling, and describe a simple, practical impedance matching network for this architecture. The resulting framework allows a system designer with a given set of circuit, device, and antenna fabrication and integration technologies to choose from a spectrum of tradeoffs between array density and RF component complexity.**

***Index Terms*—Array processing, beam steering, beamforming, millimeter-wave antenna arrays, mutual coupling, phased arrays, sigma-delta modulation.**

## I. Introduction

WHILE phased arrays are natural candidates for a wide variety of modern imaging, communication, and detection and tracking systems, their cost, size, and complexity has traditionally limited the scope of possible applications. However, advances in millimeter-wave technology in recent years hold the promise of enabling the use of phased array antennas in a host of small platform devices and portable electronics for both high-end and consumer applications. As such, there has been a resurgence of interest in practical phased array designs for such applications.

Manuscript received June 22, 2012; revised October 31, 2012; accepted November 25, 2012. Date of publication January 21, 2013; date of current version April 03, 2013. This work was supported in part by DARPA under Contract No. HR0011-06-1-0004, by the Semiconductor Research Corporation through the FCRP Center for Circuit and System Solutions (C2S2), and in part by the Department of the Air Force under Air Force Contract No. FA8721-05-C-0002. Opinions, interpretations, conclusions and recommendations are those of the authors and are not necessarily endorsed by the United States Government. This work was presented in part at the *International Symposium on Antennas and Propagation (AP/URSI)*, Toronto, Canada, July 11–17, 2010, and at the *International Symposium on Phased Array Systems and Technology*, Waltham, MA, Oct. 12–15, 2010.

J. D. Krieger and G. W. Wornell are with the Department of Electrical Engineering and Computer Science, Massachusetts Institute of Technology, Cambridge, MA 02139 USA (e-mail: ja17761@mit.edu; gww@mit.edu).

C.-P. Yeang is with the Institute for the History and Philosophy of Science and Technology, University of Toronto, ON M5S 1K7, Canada (e-mail: chenpang.yeang@utoronto.ca).

Digital Object Identifier 10.1109/TAP.2013.2241719

There continues to be progress in the development of cost-effective millimeter-wave phased arrays aimed at such applications; see, e.g., [1]–[6] and the references therein. Within the broader realm of ongoing research, some efforts are focused primarily on exploiting increasing levels of silicon integration, while other efforts primarily seek to exploit the increasing availability of inexpensive digital circuitry and processing. Moreover, some of the most promising efforts leverage both jointly.

In spite of recent progress, the components required for accurate phase control at each element in such arrays continue to be expensive, precluding the use of phased arrays in many otherwise compelling applications. Simply replacing high-end, high-resolution components with low-cost, coarsely discretized phase shifters in traditional designs sharply degrades performance, strongly limiting the quality of the beams that can be formed by the array. As a result, addressing the need for adequate phase control in beamforming remains a key challenge in the pursuit of widespread deployment of millimeter-wave phased arrays.

There has been a variety of research exploring this issue. For example, some research has focused on characterizing the capabilities of phased array systems utilizing low resolution phase shifters to meet the needs of current and proposed millimeter-wave applications [7], [8]. At the same time, other research has focused on developing novel approaches for sharing a smaller number of phase shifters (and other components) among antenna elements [9].

In this paper, we explore a rather different approach. Specifically, instead of pursuing designs with a smaller number of accurate phase shifters, we develop a high-performance architecture based on efficient utilization of a larger number of coarse phase shifters. To accomplish this, we repurpose the established theory of delta-sigma ($\Delta\Sigma$) analog-to-digital converters (ADCs) [10], applying it in the spatial domain to determine an appropriate phase for each of the densely packed elements to create a desired array pattern. In temporal domain $\Delta\Sigma$ as used in ADCs, coarsely discretized faster-than-Nyquist sampling, or *oversampling*, is used to force the quantization error to appear at higher frequencies than the original signal. This, in turn, allows the original signal to be retrieved by low-pass filtering, removing the undesired error. Exploiting a direct correspondence between temporal domain and spatial domain sampling, we observe that faster-than-Nyquist sampling in ADCs is the equivalent of sub-half-wavelength element spacing in uniform arrays. Moreover, the shaping of quantization noise into the high frequencies in ADCs is equivalent to the steering of beam pattern quantization error into the so-called invisible region of space, while leaving the intended pattern throughout the (visible) area of interest.

From a broader perspective, our architecture can be viewed as exploring potential attractive technology tradeoffs enabled by inexpensive digital processing. In particular, the architecture al-

lows for making tradeoffs between complex phase shifter design and denser antenna implementations. And with ongoing evolutions in antenna fabrication and integration technology, such tradeoffs may turn out to be quite favorable. For example, using modern lithography there is the potential to etch cost-effective dense arrays of patch antennas, which with increasing levels of density effectively become simple printed dipoles. From this perspective, the $\Delta\Sigma$ architecture represents a generalization of the traditional phased-array architecture that allows a designer, with specific implementation technology at his/her disposal, to choose from a spectrum of tradeoffs between array density on one hand, and RF circuit complexity on the other.

In the remainder of this section, we summarize some related work to provide context for the contributions of the present paper. To begin, we note that the $\Delta\Sigma$ data encoding process continues to be adapted for use in a growing number of fields and applications that exploit oversampling in the temporal domain in order to mitigate noise while using relatively simple sensors for measurement; see, e.g., [11]–[13]. Additionally, $\Delta\Sigma$ techniques have been applied to phased arrays and imaging arrays in a number of instances; see, e.g., [14]–[17]. However, these techniques have focused on the use of $\Delta\Sigma$ techniques in the more traditional temporal domain for such arrays, in contrast with our focus on exploiting spatial oversampling.

Spatial domain versions of $\Delta\Sigma$ have received attention in applications other than antenna array design; examples include image processing, wave computing, and pattern recognition [18], [19]. For instance, in the context of image processing, an approach known as error diffusion uses $\Delta\Sigma$ quantization to reproduce images from low-resolution but oversampled data. However, these methods are in the same spirit as the traditional application of $\Delta\Sigma$ principles in the temporal domain. In particular, they apply it to the data itself, whereas in our approach it is applied to the actual sensors/transducers, i.e., the antenna elements. Finally, in [20], a spatio-temporal $\Delta\Sigma$ quantization scheme is developed for transmit antenna arrays. While there are some superficial similarities to the methods we describe in the present paper, the goals are quite different, and how the $\Delta\Sigma$ methodology is exploited diverges sharply. In particular, whereas the architecture in [20] aims to reduce the temporal oversampling requirements of the time domain waveforms, ours seeks to produce specified antenna beam patterns with simpler structure and hardware.

Finally, the present paper builds on [21], in which we introduced the concept of applying spatial $\Delta\Sigma$ quantization to densely packed array elements, and [22], in which we introduced mutual coupling and impedance matching issues into the analysis. From the more comprehensive analysis of the present paper, we find, among other results, that there is a key tradeoff between pattern error and power efficiency, which can be exploited by system designers.

The remainder of the paper is organized as follows. Section II provides the required notation, terminology, concepts and background required in for our development of the dense $\Delta\Sigma$ array architecture. Section III develops our main results, describing the architecture, and characterizing its beamforming capabilities and power efficiency, taking into account mutual coupling effects and exploiting a particular efficient form of impedance matching for the architecture. Finally, Section IV concludes with a discussion of these results, their implications, and directions for future research.

## II. Array Analysis Framework

In this section, we summarize the basic antenna array concepts, terminology, notation, and perspectives specifically required for our development.

### A. Linear Array of Ideal Isotropic Elements

Consider $N$ ideal isotropic elements arranged with uniform spacing $d$ along the $z$ axis. For time-harmonic sources with angular frequency $\omega$ and associated free space wavelength $\lambda$, when the complex weights $\{w_n\}_{n=0}^{N-1}$ are applied to the array elements, the *beam pattern* in the direction given by $k_z = k\cos\theta$, where $k = 2\pi/\lambda$ is the spatial angular frequency of the waves and the angle $\theta$ is measured from the $+z$ axis, may be written as [23]

$$f(k_z) = \sum_{n=0}^{N-1} w_n e^{jnk_z d}. \tag{1}$$

The region of $k_z$-space corresponding to real values of $\theta$, $\mathcal{V} = \{k_z : |k_z| \le k\}$ is referred to as the *visible region*, or *real space*. Outside of this region, $\theta$ takes on purely imaginary values, and as such, $\mathcal{V}^{\perp}$ is referred to as *imaginary space*.

The main beam is scanned to $k_{z0}$ when a progressive phase shift across the array $\angle w_n = -nk_{z0}d$ coherently combines signals along this direction. Since the beam pattern is $2\pi/d$-periodic in $k_z$-space, the main beam direction may be uniquely specified for any $k_{z0}$ in the alias-free region $\mathcal{V}_0 = \{k_z : |k_z| \le \pi/d\}$. If $d > \pi/k$, $\mathcal{V}_0$ is a subset of $\mathcal{V}$, and it is possible to have an alias of the main beam within real space, known as a *grating lobe*.

The relative power density, or *power pattern*, of an array is given by $P(k_z) = |f(k_z)|^2$. For a transmitting array, this pattern represents the relative radiation intensity in the direction $k_z$. When a grating lobe is present in real space, a part of the power intended for the main lobe direction is instead transmitted to the grating lobe direction. For a receiving array, the power pattern gives the relative power gain of a signal arriving from $k_z$. With grating lobes, signals from unintended directions are amplified by the same level as the main lobe, leading to directional ambiguities and reduced signal-to-noise ratios.

On the other hand, when $d < \pi/k$, $\mathcal{V}_0$ extends beyond the visible region. In this case, it is possible to scan the main lobe entirely outside of real space. In the transmit case, this has the physical interpretation that the array is attempting to direct power into imaginary space, and as a consequence very little power will actually propagate away from the array. The receiving array has an analogous interpretation: it is attempting to focus on signals coming from imaginary space, thus causing any signal from real space to be combined incoherently.

With no apparent benefit gained from choosing a particularly small element spacing, conventional array design generally dictates that the spacing be set at or just slightly less than $d_0 = \pi/k = \lambda/2$. Based on this convention, a linear array with aperture length $L = Nd$ is referred to as a standard uniform

linear array when the number of elements is $N = N_0 = L/d_0$. When the same aperture is filled uniformly with more than $N_0$ elements, the resultant array is described as a dense array. As will be shown, while there is no benefit to using such an array with idealized components, a dense array has the potential to be useful for practical phased array implementation.

For our development, it is important to emphasize the distinction between the impacts of varying the array aperture size versus varying the number of array antennas, as these parameters are independently chosen in our architecture. To first order, the aperture size determines the fundamental pattern characteristics such as beamwidth and directivity. In a traditional array with element spacings near a half-wavelength, changing the aperture size is equivalent to changing the number of antennas. However, with the $\Delta\Sigma$ array architecture we focus on a fixed, but arbitrary array aperture within which the number of antennas is increased by reducing the element spacing throughout the aperture, resulting in a greater element density.

### B. Mutual Coupling

Physically, the array weights in (1) represent voltage or current excitations applied to the individual elements. For example, in an array of thin-wire dipoles, these weights are the currents across the terminals of the two dipole halves. Implicit in this expression for the beam pattern is the assumption of direct control over these terminal currents. This is known as the *forced excitation* model.

A more accurate representation of a practical array system is the *free excitation* model, characterized by the equivalent circuit shown in Fig. 1. In this model, the weights $\{w_n\}$ represent the complex voltages generated by individual sources, each with internal impedance $Z_0$. The array is described as an $N$-port network with impedance matrix $\mathbf{Z} \in \mathbb{C}^{N\times N}$ such that $\mathbf{v} = \mathbf{Z}\mathbf{i}$ [24], where $\mathbf{v}$ and $\mathbf{i}$ are length-$N$ vectors containing the voltages $\{v_n\}$ and currents $\{i_n\}$ at the terminals of the array elements. The terminal currents in Fig. 1 are related to the weights $\mathbf{w} \in \mathbb{C}^N$ according to

$$\mathbf{w} = Z_0\mathbf{i} + \mathbf{v} = (Z_0\mathbf{I} + \mathbf{Z})\mathbf{i} \tag{2}$$

where $\mathbf{I}$ is the $N \times N$ identity matrix. Defining the *coupling matrix* as $\mathbf{C} = (Z_0\mathbf{I} + \mathbf{Z})^{-1}$, such that $\mathbf{i} = \mathbf{C}\mathbf{w}$, the effects of the feed network and mutual coupling may be accounted for by replacing the $w_n$ in (1) with $i_n = \sum_{m=0}^{N-1} C_{nm}w_m$. The resultant beam pattern with mutual coupling is then

$$f^{\mathrm{MC}}(k_z) = \sum_{n=0}^{N-1}\sum_{m=0}^{N-1} C_{nm}w_m e^{jnk_z d}. \tag{3}$$

The model described above is commonly used in traditional mutual coupling analysis—see, e.g., [25]. We may obtain a useful form for the purpose of our analysis by exploiting certain structure in the coupling. In particular, it is useful to express (3) in terms of the *embedded element patterns*, which are the patterns due to a unit excitation at a specified element while in the presence of the remaining array elements. While these will vary among the elements near the edges of the array, most elements behave similarly to the elements of an infinite array.

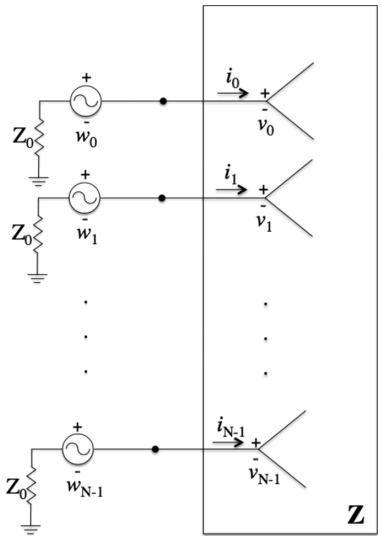


Fig. 1. Equivalent circuit diagram for the antenna array. The beamformer output is described by a set of voltage sources $\{w_n\}$, each with internal impedance $Z_0$. The mutual coupling among the array elements is modeled as a $N$-port network with impedance matrix $\mathbf{Z}$.

In the infinite array model, the physical coupling environment is constant for all elements and as such, the coupling matrix $\mathbf{C}$ has a Toeplitz structure, with identical entries along each diagonal $c_p = C_{m+p,m}$. Thus, the complete coupling matrix may be represented by the set $\{c_p\}$, which we refer to as the infinite array *coupling coefficients*. Making the substitution $p = n - m$ in (3), the beam pattern for the infinite array is

$$\begin{aligned} f^{\mathrm{MC}}(k_z) &= \sum_m \sum_p c_p w_m e^{j(m+p)k_z d} \\ &= \sum_m w_m e^{jmk_z d} \sum_p c_p e^{jpk_z d} = f(k_z)\, f_c(k_z). \end{aligned} \tag{4}$$

In (4), we have rewritten the free excitation beam pattern (3) as the product of the forced excitation beam patterns due to $\{w_m\}$ and $\{c_p\}$, the latter which we refer to as the *coupling pattern* of the array $f_c(k_z)$. From (4), we can see that the coupling pattern is the beam pattern of the array when a unit excitation is applied to the element located at the origin. Note that this is precisely the embedded pattern shared by all the array elements (up to a phase term). This useful factorization of the beam pattern allows for a convenient separation of the coupling effects from the simpler forced excitation relation used when mutual coupling is ignored.

### C. Power Efficiency

Under perfect conditions, an array will radiate all the available power delivered by the source. When the power radiated by the array $P_{\mathrm{rad}}$ is less than the incident power sent from the source $P_{\mathrm{inc}}$, the array is said to have a loss in the *power efficiency*

$$\eta = \frac{P_{\mathrm{rad}}}{P_{\mathrm{inc}}}. \tag{5}$$

If the array is composed of lossless materials, efficiency loss is due to impedance mismatches between the source and the array elements. Since the impedance of each element is the ratio of

the voltage to the current across the element terminals, mutual coupling causes these mismatches to vary with each particular array excitation.

For a particular choice of source excitations $\mathbf{w}$, the power radiated by element $n$ is $\mathrm{Re}\{i_n^* v_n\}$. The total power radiated is then

$$P_{\mathrm{rad}} = \sum_{n=0}^{N-1} \mathrm{Re}\{i_n^* v_n\} = \mathrm{Re}\{\mathbf{i}^\dagger \mathbf{v}\} = \mathbf{i}^\dagger \,\mathrm{Re}\{\mathbf{Z}\}\mathbf{i} = \mathbf{w}^\dagger (Z_0\mathbf{I}+\mathbf{Z})^{-1,\dagger}\,\mathrm{Re}\{\mathbf{Z}\}(Z_0\mathbf{I}+\mathbf{Z})^{-1}\mathbf{w}. \quad (6)$$

The power efficiency will be maximized when the array is perfectly impedance matched such that $\mathbf{v} = \mathbf{Z}\mathbf{i} = Z_0\mathbf{i}$. Hence, the total available incident power can be deduced from (6) by noting that $P_{\mathrm{inc}} = P_{\mathrm{rad}}$ when $\mathbf{Z} = Z_0\mathbf{I}$, with the result

$$P_{\mathrm{inc}} = \frac{1}{4Z_0}\mathbf{w}^\dagger\mathbf{w}. \quad (7)$$

Combining (6) and (7) with (5), we obtain, with some rearranging of terms, the following expression for the array efficiency in terms of the array excitations:

$$\eta = \frac{\mathbf{w}^\dagger(\mathbf{I}-\mathbf{S}^\dagger\mathbf{S})\mathbf{w}}{\mathbf{w}^\dagger\mathbf{w}} = 1 - \frac{\|\mathbf{S}\mathbf{w}\|^2}{\|\mathbf{w}\|^2} \quad (8)$$

where $\mathbf{S} = (Z_0\mathbf{I}-\mathbf{Z})(Z_0\mathbf{I}+\mathbf{Z})^{-1}$ is the standard *scattering matrix* of the array [24].

## III. Dense $\Delta\Sigma$ Arrays

In this section, we develop and analyze our dense array architecture.

### A. Phase Quantization

In practice, the phases of the complex array weights are restricted to some finite set of quantized values defined by the resolution of the phase shifters used in the network connecting the array to the source. Phase shifters with $M$-bits of resolution can provide any of $2^M$ values uniformly distributed over the range $[0, 2\pi)$. For a desired excitation $w_n = a_n e^{j\phi_n}$, the realized excitation is $\hat{w}_n = Q[w_n] = a_n e^{j\hat{\phi}_n}$, where the quantization operator $Q$ selects $\hat{w}_n$ such that the phase is the available value closest to $\phi_n$. As a result, there is a quantization error $q_n = \hat{w}_n - w_n$, and instead of the intended beam pattern, the array has the quantized beam pattern

$$\hat{f}(k_z) = \sum_{n=0}^{N-1} \hat{w}_n e^{jnk_z d} = \sum_{n=0}^{N-1} w_n e^{jnk_z d} + \sum_{n=0}^{N-1} q_n e^{jnk_z d}. \quad (9)$$

The first term in (9) is the desired pattern $f(k_z)$ and the second term is the pattern distortion or *quantization error pattern*

$$f_q(k_z) = \hat{f}(k_z) - f(k_z) = \sum_{n=0}^{N-1} q_n e^{jnk_z d}.$$

Traditionally, the only recourse available for reducing the pattern distortion has been to decrease the level of quantization error through the use of phase shifters with higher resolution.

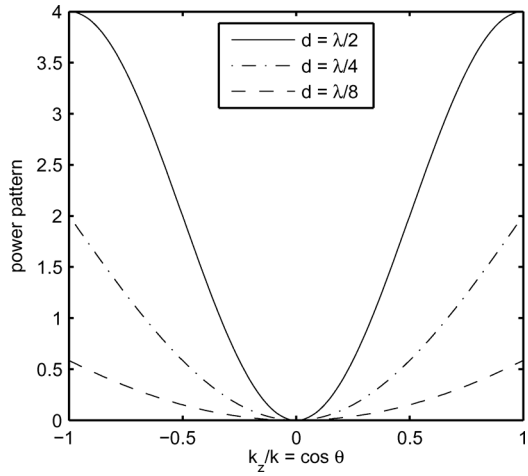


Fig. 2. Power pattern for a two-element array with excitation weights $w_0 = 1$ and $w_1 = -1$.

*1) $\Delta\Sigma$ Phase Quantization:* In the $\Delta\Sigma$ array presented in this work, the quantized phases of the array weights are determined in a different manner than in traditional arrays such that closer than typical element spacings ($d < d_0$) result in a decrease in quantization pattern distortions, even with very low resolution phase shifters. To accomplish this, the quantization error introduced at element $n-1$ is appropriately compensated by subtracting this same value from the quantizer *input* for element $n$. Thus, the $\Delta\Sigma$ quantized weight at element $n$ can be written in terms of the desired weight

$$\hat{w}_n = Q[w_n - q_{n-1}] = w_n - q_{n-1} + q_n. \quad (10)$$

By choosing the phases according to (10), every error resulting from quantization is opposed at the next element (with the exception of the final element). As the array density increases and the elements become more closely spaced, these opposing errors cancel with increasing effectiveness throughout the visible region. This cancellation technique has the additional benefit of accounting for amplitude errors, hence the amplitude of every element weight can be fixed at a constant uniform value. Thus, beyond reducing the need for precise phase control, the requirement for precise amplitude control in traditional arrays is completely removed. As such, it is important to note that for the $\Delta\Sigma$ case, the operator $Q$ differs from the previous case of direct phase quantization in that $Q[a_n e^{j\phi_n}] = \hat{a}e^{j\hat{\phi}_n}$, where $\hat{a}$ is a constant for all elements.

To understand how the close element spacing reduces pattern distortion, it is useful to consider a simple two-element array with opposing excitation weights $w_0 = 1$ and $w_1 = -1$. From (1), the beam pattern is $f(k_z) = (1 - e^{jk_z d})$. The power pattern $P(k_z) = 4\sin^2(k_z d/2)$ vanishes at $k_z = 0$ and increases monotonically to peak values at $k_z = \pm\pi/d$. For standard spacing $d = d_0 = \lambda/2$, this places the peaks at the edges of the visible region $\mathcal{V}$. In Fig. 2, the power pattern is shown in the visible region for $d = d_0$, $d_0/2$, and $d_0/4$. As the spacing is decreased, the peaks are steered outside of $\mathcal{V}$, while at the same time flattening the pattern inside. In the limit as $d \to 0$, the array becomes increasingly similar to a single antenna with

a weighting of zero and $P(k_z)$ becomes vanishingly small. In the $\Delta\Sigma$ array, the original array weights in (10) behave as intended, but the quantization *errors* combined with the purposely subtracted terms at the neighboring elements behave like this two-element array, and their contributions to the array pattern throughout real space diminishes as the spacing between elements is decreased.

As in the traditional quantization approach, the distortion in the beam pattern of the $\Delta\Sigma$ array is $f_q(k_z) = \hat{f}(k_z) - f(k_z)$. In this case, it is given by

$$f_q(k_z) = \sum_{n=0}^{N-1} (q_n - q_{n-1}) e^{jnk_z d}$$

which can be manipulated to highlight the similarity to the two-element array

$$\begin{aligned} f_q(k_z) &= \sum_{n=0}^{N-1} q_n e^{jnk_z d} - \sum_{n'=-1}^{N-2} q_{n'} e^{j(n'+1)k_z d} \\ &= (1 - e^{jk_z d}) \sum_{n=0}^{N-2} q_n e^{jnk_z d} + q_{N-1} e^{j(N-1)k_z d}. \end{aligned} \quad (11)$$

The first term in (11) shows how the $\Delta\Sigma$ array "shapes" the pattern distortions in the same way as described for the two-element array. The second term is the result of having no way to oppose the quantization error at the last element.

The $\Delta\Sigma$ noise shaping effect can be seen in the example patterns shown in Fig. 3. In these plots, the desired and $\Delta\Sigma$ quantized patterns are shown for a scan direction $k_{z0} = k/22$, with each plot representing a different element density, characterized by the array *density ratio*

$$R = \frac{d_0}{d} = \frac{N}{N_0}$$

equivalent to the oversampling ratio used in the traditional $\Delta\Sigma$ literature, which represents the increased temporal sampling rate above the standard Nyquist convention [10]. In each case, the ideal weights are specified as $w_n = ae^{-jnk_{z0}d}$, where $a$ is uniform for all elements and normalized to fix the pattern peak to unit magnitude (0 dB). The quantized weights $\hat{w}_n$ are determined according to (10) with the quantized phases limited to those of a two-bit phase shifter, thereby restricting the array element excitations to only four possible phase values. The magnitude of the quantized weights are fixed for each density ratio at $\hat{a} = 1.26a$. The choice of the relative magnitudes of $\hat{a}$ and $a$ is equivalent to the feedback level in single-loop $\Delta\Sigma$ ADCs [10], [26]. The significance of this parameter on the overall $\Delta\Sigma$ array performance will be discussed in greater detail in Section III-C. These results are consistent with the notion that the two-element patterns in Fig. 2 act as a noise shaping envelope to individual quantization errors. When $R = 1$, the most troublesome pattern distortions are not effectively shaped outside of the visible region. With $R = 2$, we can see that doubling the number of elements results in a very noticeable flattening of the quantization noise, as a great deal of the noise has now been pushed into imaginary space. With $R = 4$, the distortion within the visible region is pushed well below the level of the peak sidelobes.

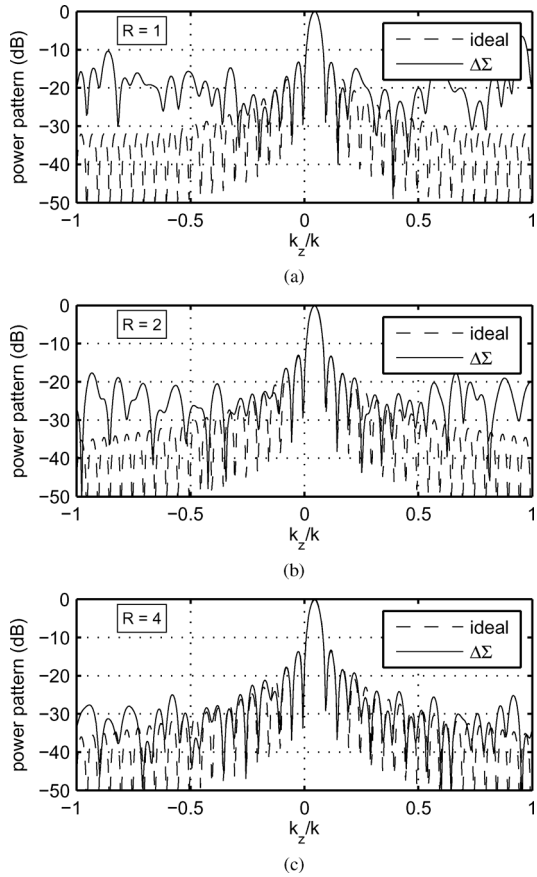


Fig. 3. Power patterns for ideal and $\Delta\Sigma$ arrays of length $L = 20\lambda$ scanned to $k_{z0} = 0.045$ k for density factors (a) $R = 1$ (b) $R = 2$ and (c) $R = 4$.

*2) $\Delta\Sigma$ Array Performance:* The signal-to-quantization-noise ratio (SQNR) is a commonly used quality measure that compares the power pattern in the desired scan direction to the average noise power distributed throughout the visible region due to the quantization errors in the array weights

$$\mathrm{SQNR} = \frac{P_{\mathrm{signal}}}{P_{\mathrm{noise}}} = \frac{P(k_{z0})}{E\left[P_q(k_z)\right]} \quad (12)$$

where $P_q(k_z) = |f_q(k_z)|^2$. Here, the expected value refers to the expected average noise power throughout the visible region, with the expectation taken over some specified distribution of array excitations. For example, if the array is to scan uniformly throughout the visible region, $P_{\mathrm{noise}}$ is the mean value of the average noise for all possible scan directions. From this definition, $P_{\mathrm{noise}}$ is equivalent to the mean squared error between the quantized and original patterns

$$P_{\mathrm{noise}} = \mathrm{MSE} = E\left[\left|\hat{f}(k_z) - f(k_z)\right|^2\right]. \quad (13)$$

Further, by scaling the array weights such that $P_{\mathrm{signal}}$ is normalized to unity, the mean squared error represents the inverse of the SQNR.

We now quantify the relationship between the MSE of the $\Delta\Sigma$ array of length $L = N_0 d_0$ and the density ratio $R$. An exact determination of this dependence requires knowledge of the various quantization errors at every element for each desired set of array weights. However, it is possible to predict this relationship analytically by modeling the quantization errors as independent and identically distributed (i.i.d.) random variables. Specifically,

$$E\left[q_m^* q_n\right] = \frac{\sigma_q^2}{N^2}\delta_{mn} \tag{14}$$

where $\sigma_q^2/N^2$ is the average noise at the individual elements (fixing $P_{\text{signal}}$), and where

$$\delta_{mn} \triangleq \begin{cases} 1 & m = n \\ 0 & \text{otherwise.} \end{cases}$$

Using this model, the expected noise power in a given direction $k_z$ can be found from (11)

$$\begin{aligned} E\left[P_q(k_z)|k_z\right] &= \left|1 - e^{jk_z d}\right|^2 \sum_{n=0}^{N-2} \frac{\sigma_q^2}{N^2} + \frac{\sigma_q^2}{N^2} \\ &= \left(2(1-\cos k_z d)(N-1)+1\right)\frac{\sigma_q^2}{N^2}. \end{aligned} \tag{15}$$

The predicted MSE is found by calculating the average of (15) over the visible region

$$\begin{aligned} \text{MSE} &= \frac{1}{2k}\int_{-k}^{k} E\left[P_q(k_z)|k_z\right] dk_z \\ &= \frac{1}{2k}\left[2\left(k_z - \frac{1}{d}\sin k_z d\right)(N-1) + k_z\right]\Bigg|_{-k}^{k} \frac{\sigma_q^2}{N^2} \\ &= \left(2\left(1 - \frac{\sin kd}{kd}\right)(N-1)+1\right)\frac{\sigma_q^2}{N^2}. \end{aligned} \tag{16}$$

In the limiting case, as $d \ll \pi/k$, we use the small angle approximation $\sin x \approx x - x^3/6$ to obtain

$$\text{MSE} = \left(\frac{k^2 d_0^2}{3N_0}\frac{N-1}{N}\frac{1}{R^3} + \frac{1}{N_0^2}\frac{1}{R^2}\right)\sigma_q^2. \tag{17}$$

In this form, we see that the contribution to the MSE from the first $N-1$ quantization errors and their counterparts should decrease with $R^3$. The contribution from the final element decreases with $R^2$ due to the reduced portion of the total power provided to that element as the array density grows. In principle, as $R$ grows very large, the effect of the $\Delta\Sigma$ cancellations will continue to eliminate the noise due to the rest of the array to the point that the noise caused by this single element becomes the dominant source of quantization noise. However, in nearly all practical settings this edge contribution will be negligible. As an example, for an array of length $L = 2\lambda$ ($N_0 = 4$), a density ratio of $R = 12.9$ is required for the two terms in (17) to be comparable in magnitude.

Exact values of the MSE were determined numerically over a range of density ratios for the case of a linear array of ideal isotropic elements of length $L = 20\lambda$, designed to scan uniformly throughout real space with uniform amplitude weighting for all elements. At each value of $R$, the MSE was calculated directly from (13) by averaging the noise power over the visible region for each scan angle, then evaluating the mean value over all scan angles. In addition, the predicted MSE in (17) was calculated from the resultant sample values of $\sigma_q^2$ for each $R$. With the array weights properly normalized, the MSE results were inverted, yielding the simulated and predicted SQNR at each $R$, as depicted in Fig. 4, which shows close agreement between the two curves.

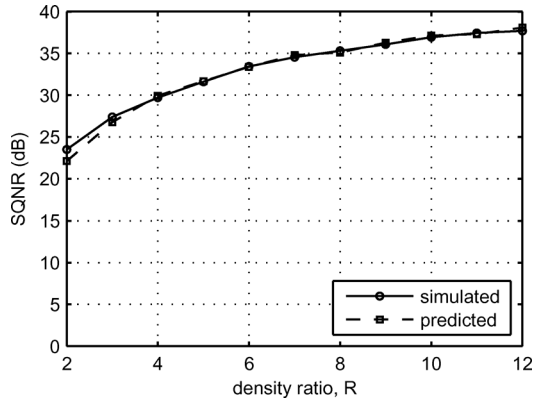


Fig. 4. $\Delta\Sigma$ SQNR results for uniform amplitude scanning array of length $L = 20\lambda$.

TABLE I
SQNR RESULTS FOR UNIFORM AMPLITUDE SCANNING ARRAYS OF LENGTH $L = 20\lambda$ USING DIRECT PHASE QUANTIZATION WITH $M$ BITS OF PHASE RESOLUTION WITH EQUIVALENT $\Delta\Sigma$ DENSITY RATIOS $R_{\text{equiv}}$

| $M$ | SQNR (dB) | $R_{\text{equiv}}$ |
|---|---|---|
| 2 | 23.1 | 1.9 |
| 3 | 28.8 | 3.6 |
| 4 | 35.2 | 7.6 |

Similar MSE calculations were performed for a standard linear array of the same length assuming phase shifters with $M = 2$, 3, and 4 bits of resolution. The results are summarized in Table I, along with the corresponding density ratios $R_{\text{equiv}}$ required to obtain the same SQNR values with the two-bit $\Delta\Sigma$ array. These results match quite closely to the relationship

$$R_{\text{equiv}} = 0.47 \cdot 2^M \tag{18}$$

which provides a sense of how the appropriate $\Delta\Sigma$ density ratio should be selected to match the performance associated with specified number of phase shifter bits in a conventional array.

### B. Mutual Coupling Effects

In the design of a dense array, the close proximity of the elements makes it particularly important to understand and account for the effects of mutual coupling. The results presented in Section III-A were determined based on the forced excitation model. We now will consider the more realistic free excitation model and determine whether the $\Delta\Sigma$ array continues to perform as desired. Following the analysis approach described in Section II-B, we first consider the infinite array case and treat the edge effects due to finite array lengths separately.

Recall from (4) that under the free excitation model, the beam pattern of the infinite array can be decoupled into the product of

the corresponding forced excitation pattern $f(k_z)$ and the coupling pattern $f_c(k_z)$, which is an inherent property of the array, independent of the particular excitations. Consequently, the $\Delta\Sigma$ beam pattern in any direction $\hat{f}^{\mathrm{MC}}(k_z)$ may be thought of as the $\Delta\Sigma$ beam pattern analyzed in Section III-A multiplied by a proportionality constant given by the coupling pattern. From this viewpoint, the interactions among the array elements – regardless of spacing – should have a problematic effect only if $f_c(k_z)$ generally tends to be of greater magnitude in the regions of real space for which the $\Delta\Sigma$ pattern distortions are the most extreme, that is, towards larger values of $|k_z|$. Further, the likelihood of this being the case may be addressed intuitively by considering the forced excitation idealization as a special case of the free excitation model with coupling coefficients $c_p = \delta_{p,0}$, corresponding to $f_c(k_z) = 1$. More generally, we expect $c_p$ to decay smoothly with $|p|$. Based on a standard result from Fourier analysis, this more gradual decay of the coupling coefficients implies that $f_c(k_z)$ should decrease away from the origin, unlike the "flat" coupling pattern associated with forced excitation model. This observation suggests that mutual coupling has the effect of actually *suppressing* the most troublesome pattern distortions located near the extents of the visible region.

To simulate the effects of mutual coupling, the model given by Wasylkiwskyj *et al.* [27] for the mutual impedance of two thin-wire dipole antennas was used. In this model, the system impedance is normalized such that $Z_0 = 1$ and the impedance matrix entries are given by

$$Z_{mn} = \begin{cases} 1 & m = n \\ H_0^{(2)}(kd|n-m|) & m \neq n, \end{cases} \tag{19}$$

where $H_0^{(2)}(\cdot)$ is the zeroth-order Hankel function of the second kind. While the analysis in [27] is specific to the case of two isolated thin-wire dipoles, the results apply rather directly to our array setup. Indeed, the presence in the array environment of the additional open-circuited dipoles in the determination of the impedance matrix elements has negligible effect as the two separated dipole halves are far from resonant and appear relatively transparent to the electromagnetic fields.

Using (19), the coupling matrix $\mathbf{C}$ was determined for the array of length $L = 20\lambda$ with density ratio $R = 4$. For an array of this size, the entries of the coupling matrix corresponding to an element near the center of the array are nearly identical to the non-trivial coupling coefficients $\{c_p\}$ of an infinite array element. The magnitudes of these values $|c_p|$ are shown in Fig. 5(a) versus the element separation index $p$. The associated coupling pattern $f_c(k_z)$ is shown in Fig. 5(b), in which we see the expected decrease away from the origin, with particularly sharp drop-offs beyond $|k_z/k| = 0.9$.

To illustrate the overall effect of mutual coupling, the pattern calculations performed to create Fig. 3 were repeated based on the free excitation model using (3) with coupling matrix entries determined by (19). The quantization error patterns for both the forced and free excitation models, $f_q(k_z)$ and $f_q^{\mathrm{MC}}(k_z)$, are shown in Fig. 6 for $R = 1$, 2, and 4. In each of the three cases, the distortion near the edges of the visible region, where $\Delta\Sigma$ noise shaping alone is least effective, is decreased when the calculation accounts for mutual coupling, as implied by Fig. 5(b).

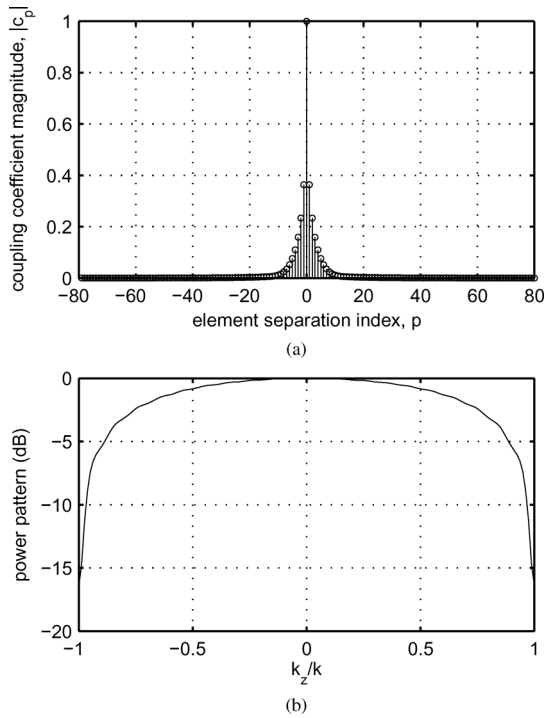


Fig. 5. (a) Magnitude of the coupling coefficients $\{c_p\}$ for a central element in an array of length $L = 20\lambda$, with $R = 4$. (b) Beam pattern response $f_c(k_z)$ for an array excited by the coupling coefficients.

While the infinite array analysis explains the effect of mutual coupling near the edges of visible space, the slight increase in the pattern distortion near the origin seen in the case of $R = 4$, for example, is not accounted for by this approach, as the infinite array analysis predicts no modification along this direction. From this observation, we may surmise that edge effects have slightly greater significance due to mutual coupling. This result is unsurprising since in the case of the finite array, the embedded element patterns in actuality exhibit more variations for the elements near the array edges. As a result, the opposing $\Delta\Sigma$ quantization errors do not cancel quite as effectively as elements with identical embedded patterns. However, these effects appear to be relatively benign, appearing only when the pattern distortion is decreased to about 30 dB below the main lobe level.

When the SQNR calculations used to generate Fig. 4 are repeated for the free excitation model, the results are as shown in Fig. 7. The simulated results for the forced excitation model are also shown to illustrate that the effects of coupling add only a small amount of additional error, consistent with the above discussion.

### C. $\Delta\Sigma$ Power Efficiency

The power efficiency of the $\Delta\Sigma$ array is affected by both the increased array density and the unique nature of the $\Delta\Sigma$ excitations. We begin with a description of a simple yet effective approach for maintaining acceptable array efficiencies for general dense scanning arrays, and then apply this concept specifically to the $\Delta\Sigma$ array.

*1) Impedance Matching for Dense Arrays:* Impedance mismatch losses can be reduced by placing a matching network between the source and the array. For a single antenna, a perfect match may be obtained by using a series reactance and

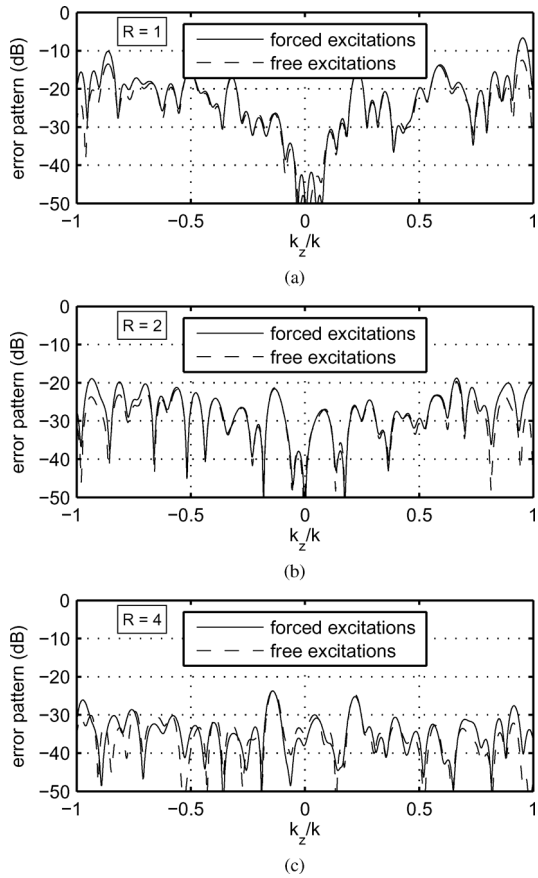


Fig. 6. Quantization error (power) patterns for the $\Delta\Sigma$ array of length $L = 20\lambda$ using both the forced and free excitation models with density ratios (a) $R = 1$ (b) $R = 2$ and (c) $R = 4$.

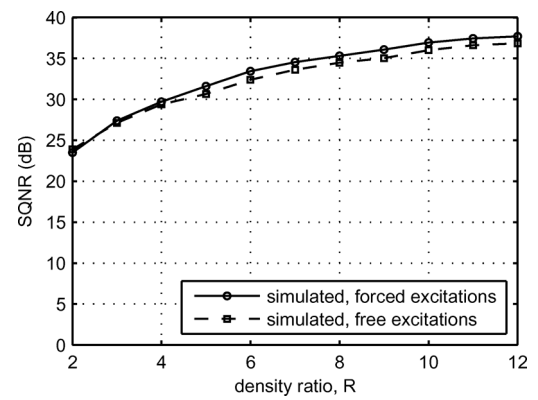


Fig. 7. Comparison of SQNR versus density ratio $R$ for $\Delta\Sigma$ arrays based on the forced and free excitation models. $L = 20\lambda$.

a quarter-wavelength of transmission line to match the imaginary and real parts of the antenna impedance, respectively, to the source impedance. With a phased array, the presence of mutual coupling makes matching much more complicated, necessitating the use of complex matching networks to avoid efficiency losses. Examples include the use of dynamically varying components that modify the network characteristics for every set of array excitations or a web of interconnections between the array elements. A far more practical alternative is based on the notion of *scan impedance*, defined as the effective impedance (sometimes referred to as the active impedance) of each element when scanned to a particular direction $k_{z0}$ [28]

$$Z_n^{\text{scan}}(k_{z0}) = \frac{v_n(k_{z0})}{i_n(k_{z0})}. \tag{20}$$

For the particular set of excitations corresponding to scan angle $k_{z0}$, it follows that $\mathbf{v}(k_{z0}) = \mathbf{Z}\,\mathbf{i}(k_{z0}) = \mathbf{Z}^{\text{scan}}(k_{z0})\mathbf{i}(k_{z0})$, where $\mathbf{Z}^{\text{scan}}(k_{z0})$ is a diagonal matrix with entries given by (20). Because of this, the scattering matrix at this scan angle can also be replaced by substituting $\mathbf{Z}$ with $\mathbf{Z}^{\text{scan}}(k_{z0})$ such that

$$\mathbf{S}^{\text{scan}}(k_{z0}) = \left(Z_0\mathbf{I} - \mathbf{Z}^{\text{scan}}(k_{z0})\right)\left(Z_0\mathbf{I} + \mathbf{Z}^{\text{scan}}(k_{z0})\right)^{-1}. \tag{21}$$

Since for each scan angle the matrix in (21) is diagonal, it may be decoupled into $N$ scalar equations of the form

$$\Gamma_n^{\text{scan}}(k_{z0}) = \frac{Z_0 - Z_n^{\text{scan}}(k_{z0})}{Z_0 + Z_n^{\text{scan}}(k_{z0})} \tag{22}$$

with the *scan reflection coefficient* $\Gamma_n^{\text{scan}}(k_{z0})$ for element $n$ (at scan angle $k_{z0}$) corresponding to the $n$th diagonal entry of $\mathbf{S}^{\text{scan}}(k_{z0})$. This term captures the effective ratio of the signal returned back along the feed line to the original signal $w_n$. Because the scan reflection coefficient is a function of $Z_n^{\text{scan}}(k_{z0})$, which includes the effects of coupling for all $N$ array elements, this reflection is in reality a superposition of both the incident signal at the element as well as the coupled signals from the other $N-1$ elements. As such, (8) can be expressed as the array *scan efficiency*

$$\begin{aligned}\eta^{\text{scan}}(k_{z0}) &= 1 - \frac{\left\|\mathbf{S}^{\text{scan}}(k_{z0})\mathbf{w}(k_{z0})\right\|^2}{\left\|\mathbf{w}(k_{z0})\right\|^2} \\ &= 1 - \frac{\sum_{n=0}^{N-1}\left|\Gamma_n^{\text{scan}}(k_{z0})w_n(k_{z0})\right|^2}{\sum_{n=0}^{N-1}\left|w_n(k_{z0})\right|^2}.\end{aligned} \tag{23}$$

Using the scalar equivalent for the element impedance in (20), it is possible to match each element such that $Z_n^{\text{scan}}(k_{z0}) = Z_0$ in the same way one would match a single antenna. However, since this scan impedance is only valid at $k_{z0}$, when the beam is scanned to any other angle, the change in scan impedance results in a loss of efficiency. As element spacing decreases, it is to be expected that mutual coupling effects become more prevalent, yet these effects are not necessarily disadvantageous to the power efficiency. In fact, as the array scans from one direction to another, the incremental phase change between neighboring elements is inversely proportional to their spacing, and thus we can expect the scan impedance to be *less* sensitive to changes in the scan direction. This motivates the use of *scan impedance matching*, in which the array is matched to the scan impedance in one specified direction. This sub-optimal matching technique is applied with the expectation that the scan impedance does not vary greatly over the entire range of potential scan angles. Based on the above observation, this implies that this very simple approach is particularly well suited for use with dense arrays.

To develop the idea, the scan impedance matching approach was applied to an array of length $L = 20\lambda$ using the impedance

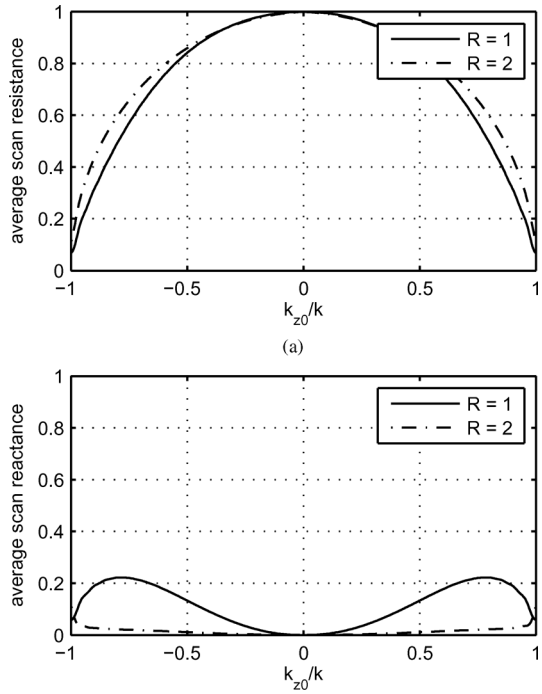


Fig. 8. (a) Real part and (b) imaginary part of the average scan impedance of elements in an array of length $L = 20\lambda$, for density ratios $R = 1$ and $R = 2$. Calculations include scan impedance matching network designed for perfect match to $Z_0 = 1$ at $k_{z0} = 0$.

matrix values obtained from (19) for several density ratios. The scan impedances of the unmatched array elements were calculated using (20) for the broadside scan direction of the array, $k_{z0} = 0$, and an individual matching network consisting of a series reactance and a quarter-wave transmission line was applied at each element to match these impedances to the normalized system impedance $Z_0 = 1$. The resulting average matched scan impedances are shown in Fig. 8 for both a standard ($R = 1$) and dense ($R = 2$) array. At $k_{z0} = 0$, both arrays have scan impedances with real parts equal to the system impedance $Z_0$ and zero imaginary parts, corresponding to a perfect match. However, away from broadside, the standard array scan impedance exhibits a greater sensitivity to changes in scan angle than seen for the dense array, as expected.

*2) Efficiency Effects Due to $\Delta\Sigma$ Weights:* In addition to the effect of the increased element density on the power efficiency, we must consider the effect of using the $\Delta\Sigma$ weights instead of the ideal array weights. In particular, we characterize the fractional reduction of the $\Delta\Sigma$ array efficiency $\hat{\eta}$ from the efficiency $\eta$ of the equivalent array excited by ideal (unquantized) weights

$$\rho = \frac{\eta}{\hat{\eta}}. \tag{24}$$

Consider an array with the matching network in place, some set of ideal weights $\{w_n\}$ with associated $\Delta\Sigma$ weights $\{\hat{w}_n\}$, and assume that the array is sufficiently dense such that the beam patterns are nearly identical. Since the total power radiated is proportional to the power pattern integrated over real space, it follows that $\hat{P}_{\rm rad} \approx P_{\rm rad}$. To obtain similar patterns, the ratio of the magnitudes of the $\Delta\Sigma$ weights to those of the ideal weights, $\gamma = \hat{a}/a$, must be greater than unity in order to steer the pattern distortions into imaginary space. Therefore, from (7) it follows

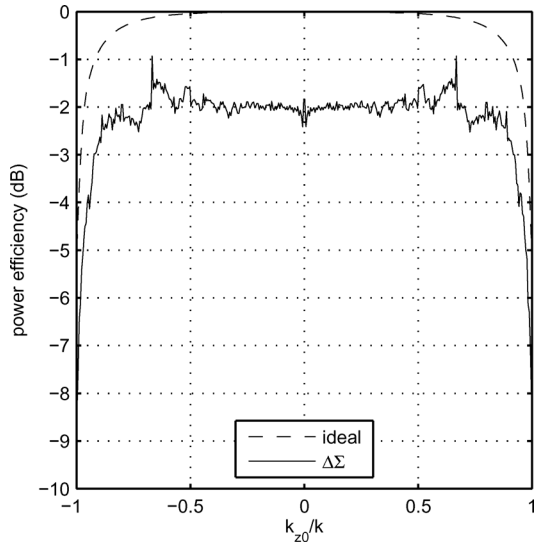


Fig. 9. Power efficiency as a function of scan angle $k_{z0}$, $L = 20\lambda$, $R = 4$, with scan impedance matching network designed for perfect match at $k_{z0} = 0$. Results for the $\Delta\Sigma$ array obtained by setting $\hat{a} = 1.26a$ such that the nominal efficiency is within approximately 2 dB of the ideal result.

that $\hat{P}_{\rm inc} > P_{\rm inc}$. Using the definition of the power efficiency in (5), we can estimate the efficiency loss in the case of low pattern noise as

$$\rho_{\rm est} = \frac{\hat{a}^2}{a^2} = \gamma^2 > 1. \tag{25}$$

Put simply, the $\Delta\Sigma$ excitations as expressed in (10) radiate the same amount of power as in the case of the ideal excitations due to the $w_n$ terms, while the quantization terms $q_n$ radiate zero power once their beam pattern contributions are effectively steered from real space. Hence, we can expect the efficiency of the $\Delta\Sigma$ array to be less than that of an identical array excited with ideal weights. The exact amount depends on the choice of $\gamma$, which as we will discuss shortly, also plays a role in how quickly the $\Delta\Sigma$ pattern converges to the desired pattern.

For example, in the patterns and SQNR results presented thus far, the $\Delta\Sigma$ weights were determined by setting $\gamma = 1.26$. When the quantization noise is relatively small, such as in Fig. 3(c), the power radiated using both the ideal and $\Delta\Sigma$ weights is nearly identical, while the total power incident on the array is a factor of $\gamma^2 \approx 1.59$ greater in the $\Delta\Sigma$ case.

Equation (25) implies we should expect to see a reduction in the $\Delta\Sigma$ power efficiency of $\gamma^2$, corresponding to a 2 dB power efficiency loss. Exact efficiency results calculated for $R = 4$ are shown as a function of scan angle for both the ideal and the $\Delta\Sigma$ weights in Fig. 9. These results were calculated directly from (8) with a scan impedance match network tuned to a perfect match for the ideal weights at $k_{z0} = 0$. We first note from the ideal excitation results that the scan impedance matching works quite well for the dense array, with nearly negligible efficiency losses for scan angles throughout the region $|k_{z0}| \leq 0.5k$ (corresponding to $\pm 60^\circ$ from the array broadside). Further, the predicted power efficiency reduction of 2 dB shows a very good agreement with the $\Delta\Sigma$ array results. The fluctuations seen in the $\Delta\Sigma$ results are due to varying levels of pattern noise for different scan angles, which affect the assumption that the radiated power is equal to that of the ideal weights. Similar calculations

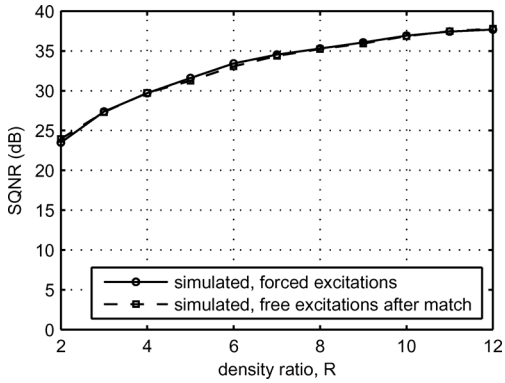


Fig. 10. SQNR dependence on density ratio $R$ for $\Delta\Sigma$ arrays using forced excitations and free excitations with matching network designed for ideal match at $k_{z0} = 0$. Array length $L = 20\lambda$.

for increased density ratios had less variations, since the quantization noise was lower throughout the visible region.

Inclusion of a matching network has the additional effect of altering the coupling matrix $\mathbf{C}$ relating the free excitations to the currents across the terminals of the array elements as described in Section II-B. As such, it is necessary to revisit the SQNR performance of the $\Delta\Sigma$ array to reflect these changes. Analysis of the combined network yields the matched coupling matrix

$$\mathbf{C}_M = -j\left(\mathbf{Z}_t + Z_0\mathbf{Z}_t^{-1}(\mathbf{Z} - j\mathbf{X}_s)\right)^{-1}$$

where $\mathbf{Z}_t$ is a diagonal matrix containing the characteristic impedances of the quarter-wave transmission lines used to match the real part of the element impedances and $\mathbf{X}_s$ is a diagonal matrix containing the reactances of the components used to match the imaginary part of the element impedances. A derivation is provided in the Appendix.

When the matched coupling matrix is used in place of the original coupling matrix in the SQNR calculations, the results are as shown in Fig. 10. Interestingly, the matching network appears to have the added benefit of improving the ability of the $\Delta\Sigma$ array to produce desired beam patterns. Closer inspection of the embedded element patterns with and without the matching network verifies that the matched array embedded element patterns show considerably less variation near the edge of the array than in the unmatched case. This observation supports the earlier conjecture that such variations were responsible for the slight decrease in the SQNR for the unmatched free excitations seen in Fig. 7.

Based on (25), it may be tempting to select an arbitrarily low value for $\gamma$ in order to minimize efficiency losses. However, since this estimate is obtained by assuming that $\hat{P}_{\rm rad} = P_{\rm rad}$, it is necessary to determine the array efficiencies directly from (8) to obtain the exact dependence of $\rho$ on the choice of $\gamma$. Exact values of $\rho$ were calculated for different density ratios $R$ with the value of $\gamma$ varying from 1 to $\sqrt{2}$ (0 to 3 dB estimated power efficiency loss). Fig. 11 shows the resulting nominal value of $\rho$, averaged over uniformly distributed scan angles, over the range of $\gamma$. These results demonstrate that as $\gamma$ approaches unity, the exact efficiency loss values are quite different that the estimated loss found using (25). This indicates not only that the efficiency loss cannot be made arbitrarily small, but also that small values of $\gamma$ result in greater pattern distortion, thereby affecting the SQNR as well as $\rho$.

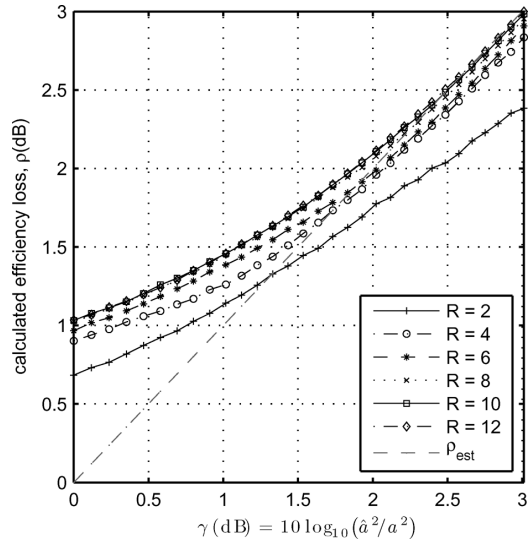


Fig. 11. Nominal power efficiency loss versus the ratio of the $\Delta\Sigma$ and ideal array weight magnitudes $\gamma = \hat{a}/a$. The dashed grey line shows the corresponding estimated value of $\rho$ given by (25).

The results in Fig. 11 also demonstrate that the relationship between the $\Delta\Sigma$ array efficiency and $\gamma$ depends on the particular value of $R$. Specifically, the value of $\gamma$ at which each curve intersects with the estimated result increases with $R$, implying that it may be necessary to accept additional efficiency loss to obtain the maximum achievable SQNR as the density ratio of the $\Delta\Sigma$ array is increased. This interpretation is verified by the results shown in Fig. 12, in which the SQNR for the $L = 20\lambda$ array is plotted against the efficiency loss $\rho$ as $\gamma$ is varied over the same range as in Fig. 11 for a number of density ratios. The horizontal dashed grey line shows the SQNR of a standard array of the same length utilizing the same two-bit phase shifters used in the $\Delta\Sigma$ array. As would be expected, this value represents a lower bound on the $\Delta\Sigma$ results for low density ratios. The asymptotic limit shared by all values of $R$ as $\rho$ decreases, shown by the slanted light grey dashed line, represents the maximum signal-to-quantization-noise level $\mathrm{SQNR}_\rho^{\max}$ that can be obtained for a specified efficiency loss, regardless of how large the density ratio is. Comparison of the results in Fig. 12 with those generated for other array lengths show both dashed lines having a vertical shift proportional to the fractional change in length. This is to be expected, based simply on the linear change in the number of elements in both cases. Since the vertical shift maintains the slope of the line representing the $\mathrm{SQNR}_\rho^{\max}$, found by a linear fit to be $\Delta\mathrm{SQNR}_\rho^{\max}(\mathrm{dB})/\Delta\rho(\mathrm{dB}) = 10.8$, we may express the dependence of $\mathrm{SQNR}_\rho^{\max}$ on both $\rho$ and $L$ (in linear scale) as

$$\mathrm{SQNR}_\rho^{\max} = 2.3\rho^{10.8}L. \tag{26}$$

Similarly, we define $\mathrm{SQNR}_R^{\max}$ as the maximum SQNR achievable for a given density ratio. This can be expressed in a similar fashion as in (26), i.e.,

$$\mathrm{SQNR}_R^{\max} = cR^\alpha L$$

for some $c$. However, the complex dependence on the array edge effects, the specific value of $\gamma$, and a constraint on the efficiency

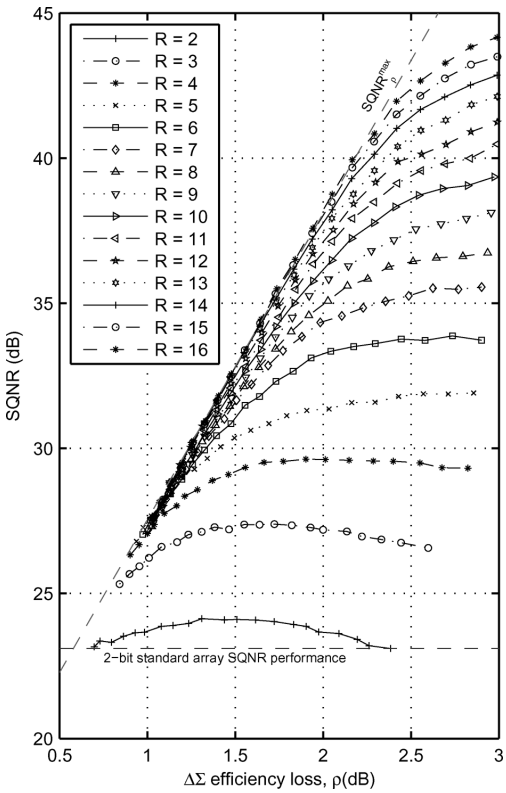


Fig. 12. SQNR versus power efficiency loss for the length $L = 20\lambda$ array.

loss to somewhat reasonable values given by $\rho \leq 2$ causes the exponent $\alpha$ to vary from about 2 at lengths of just a few wavelengths to about 2.5 at $L = 20\lambda$, increasing slowly for greater lengths. A more appropriate indication of the behavior of $\mathrm{SQNR}_R^{\max}$ can be found by inverting the MSE relation given by (17), in which the array length $L = N_0 d_0$ and associated edge effects are treated explicitly, while the effect of $\gamma$ is captured by the average quantization excitation noise $\sigma_q^2$. From simulated results, at lengths greater than $L = 4\lambda$, the calculated value of $\mathrm{SQNR}_R^{\max}$ is closely approximated using the result given by (17) with $\sigma_q^2 = 0.9$.

While the particular aspects of the intended application of any system ultimately governs the relative value of such important metrics as hardware costs, pattern precision, and power efficiency, the results shown in Fig. 12 clearly suggest that each particular density ratio has some range of natural operating points, outside of which the tradeoff required to improve one metric requires an unreasonable sacrifice with regard to the other. As an example, consider the curve corresponding to $R = 4$ at the point where $\rho = 1.4$ dB. In the neighborhood surrounding this operating point, the choice of $\gamma$ may be adjusted to accommodate an improvement in either the SQNR or the power efficiency at a reasonable cost with regard to the other. However, such costs increase rapidly as the curve approaches either of the maximum SQNR asymptotes described above. As such, if it appears necessary to operate near one of these boundaries, this simply suggests that selecting an alternative density ratio is likely to be a more efficient use of resources. Several candidate designs for $R = 2$ to $R = 6$ are illustrated in Table II in which the particular choices of $\gamma$ correspond to operational points close to the center of this natural tradeoff range for each density ratio.

TABLE II
COMPARISON OF SEVERAL ARRAY CONFIGURATIONS FOR $\Delta\Sigma$ ARRAYS OF LENGTH $L = 20\lambda$

| $R$ | $N$ | $\gamma$ | SQNR (dB) | $\rho$ (dB) |
|---|---|---|---|---|
| 2 | 80 | 1.07 | 23.6 | 0.9 |
| 3 | 120 | 1.09 | 26.8 | 1.2 |
| 4 | 160 | 1.15 | 28.9 | 1.4 |
| 5 | 200 | 1.19 | 30.7 | 1.6 |
| 6 | 240 | 1.23 | 32.6 | 1.8 |

## IV. DISCUSSION AND CONCLUDING REMARKS

Our results demonstrate the ability of a dense $\Delta\Sigma$ array to create a desired beam pattern using low-resolution two-bit phase shifters. The dependence of the signal-to-quantization-noise ratio on the density ratio agrees quite well with predicted analytical results based on an i.i.d. model for the $\Delta\Sigma$ quantization errors. This is consistent with the analysis in [10] for conventional $\Delta\Sigma$ data conversion up to an edge effect due to the finite extent of the array aperture.

Other considerations unique to this novel application of $\Delta\Sigma$ quantization covered in this work are the effects of mutual coupling and power efficiency. The adverse consequences of mutual coupling appear to be limited to mild amounts of additional pattern distortion due to the variations in the embedded element patterns near the edge of the array. When the array is connected to a matching network for the purpose of improving the power efficiency, this network modifies the overall coupling behavior of the array in a way that results in less embedded element pattern variation, providing the added benefit of decreasing the pattern error caused by mutual coupling in the unmatched case. Mutual coupling also provides the positive effect of adding a second "shaping" of the quantization pattern noise that further suppresses much of the troublesome pattern distortion near the extents of the visible region.

We see that the power efficiency of the $\Delta\Sigma$ array is, in general, less than an equivalent array excited with ideal unquantized weights, but that the degree to which the efficiency is reduced can be specified in the selection of the array weights, with a tradeoff between the SQNR and the resultant efficiency. The results indicate that, with two-bit phase shifters, for a modest density ratio of, say, $R = 4$, we can expect an improvement in SQNR of approximately 6 dB relative to a conventional array using the same low resolution components, while limiting the efficiency losses to about 1.5 dB below the array utilizing infinitely precise phase controls. With respect to power efficiency, we also demonstrated that the particularly simple scan impedance matching approach allowed us to accommodate the high coupling levels inherent in a densely packed phased array.

It is also worth emphasizing a finer grain analysis of beamforming accuracy of the $\Delta\Sigma$ array performance is typically desired. In particular, while the calculation of the SQNR via our definition of the MSE captures the gross characteristics of the beam pattern, in practice a more detailed characterization of the scanning accuracy, sidelobe behavior, and beamwidth are often required. Indeed, even when the MSE adequately captures scanning accuracy and beamwidth performance, the presence of large sidelobes due specifically to quantization noise may not be revealed by this measure if they occur in a limited number

of scan directions. We note, however, that while not explicitly developed in this paper, calculations of average and maximum sidelobe levels over the same range of scan directions used to calculate the SQNR results found worst-case sidelobe increases over the ideal case of a small fraction of a dB.

More broadly, it is also worth emphasizing that, as discussed at the outset of the paper, since the dense $\Delta\Sigma$ architecture is a generalization of the traditional architecture, it should be viewed not as an alternative to the traditional architecture, but rather as a framework for enabling tradeoffs between available circuit, device, and antenna technologies. From this perspective, the results provide useful guidelines for systems designers given various cost constraints and other resources.

Beyond the developments of the present paper, some of our further investigation has suggested additional potential advantages of the proposed architecture. For example, although this paper has focused on the specific case of uniform amplitude scanning arrays, phased arrays can be used in many other ways when both the amplitude and phase are allowed to vary dynamically. In conventional designs, this introduces a whole additional requirement for accurate amplitude control necessitating the use of the highly-linear power amplifiers. With the $\Delta\Sigma$ array, the same mechanism discussed in this paper can replicate the beam pattern of arbitrary amplitudes as well as arbitrary phases while in fact the amplitude is uniform for every element, completely eliminating the need for individual amplitude control. For such applications, the analysis provided in this paper will be particularly useful.

Finally, yet another compelling motivation for exploring the $\Delta\Sigma$ array architecture stems from its potential to provide improved robustness, which we are also only beginning to develop. In particular, an important issue in traditional array design is the sensitivity to gain and phase errors and to imprecise positioning of the individual elements. Such considerations are of increasing concern with the growing interest in using phased arrays in any handheld or otherwise mobile devices. Conveniently, such sensitivities are naturally mitigated to some degree when the number of antennas is large, such as in the case of dense arrays. Further, dense arrays typically have greater operational bandwidth for reasons roughly analogous to the relationship between the scan impedance and element spacing described in Section III-C. Though such additional research is ongoing, we speculate that a $\Delta\Sigma$ dense array can yield improved wideband performance compared to a conventional array of similar antenna elements, even after accounting for the incurred 1–2 dB efficiency reduction also described Section III-C. Hence, the $\Delta\Sigma$ array holds the promise of leading to particularly cost effective designs, relative to what is possible with standard arrays.

## Appendix
## Matched Array Coupling Matrix Derivation

Referring to Fig. 1, the matching network at element $n$ is introduced by connecting a quarter wavelength transmission line with characteristic impedance $Z_{tn}$ to source $w_n$, followed by a series reactance $-jX_{sn}$, which in turn connected to the antenna terminals. Following standard microwave network analysis (see, e.g., [24] for additional details), the voltage and current at the input to the network are related to the voltage and current at the antenna terminals by

$$\begin{aligned} v_n^{in} &= jZ_{tn}i_n \\ i_n^{in} &= jZ_{tn}^{-1}(v_n - jX_{sn}i_n), \end{aligned}$$

and to the source excitations by

$$w_n = v_n^{in} + Z_0 i_n^{in}. \tag{27}$$

Letting $\mathbf{w}$, $\mathbf{v}^{in}$, $\mathbf{i}^{in}$, $\mathbf{v}$, and $\mathbf{i}$ be length-$N$ complex vectors associated with the above scalar quantities, and similarly organizing the match network quantities into $N \times N$ diagonal matrices $\mathbf{Z}_t$ and $\mathbf{X}_s$, these relations may be combined to include the complete array

$$\begin{aligned} \mathbf{v}^{in} &= j\mathbf{Z}_t\mathbf{i}, \\ \mathbf{i}^{in} &= j\mathbf{Z}_t^{-1}(\mathbf{v} - j\mathbf{X}_s\mathbf{i}), \\ \mathbf{w} &= \mathbf{v}^{in} + Z_0\mathbf{i}^{in}. \end{aligned}$$

As the matching network will not effect the impedance relations occurring outside of the array, the original impedance relation $\mathbf{v} = \mathbf{Z}\mathbf{i}$ remains valid. Using this additional relationship, we can make the following operations

$$\begin{aligned} \mathbf{w} &= j\mathbf{Z}_t\mathbf{i} + jZ_0\mathbf{Z}_t^{-1}(\mathbf{v} - j\mathbf{X}_s\mathbf{i}) \\ &= j\left(\mathbf{Z}_t + Z_0\mathbf{Z}_t^{-1}(\mathbf{Z} - j\mathbf{X}_s)\right)\mathbf{i}. \end{aligned}$$

Having eliminated all other voltage and current terms, this last expression may be rewritten as $\mathbf{i} = \mathbf{C}_M\mathbf{w}$, where

$$\mathbf{C}_M = -j\left(\mathbf{Z}_t + Z_0\mathbf{Z}_t^{-1}(\mathbf{Z} - j\mathbf{X}_s)\right)^{-1}. \tag{28}$$

## References


[1] S. Lin, K. Ng, H. Wong, K. Luk, S. Wong, and A. Poon, "A 60 GHz digitally controlled RF beamforming array in 65 nm CMOS with off-chip antennas," presented at the IEEE Radio Frequency Integrated Circuits Symp. (RFIC), Jun. 2011.

[2] H. Krishnaswamy, A. Valdes-Garcia, and J.-W. Lai, "A silicon-based, all-passive, 60 GHz, 4-element, phased-array beamformer featuring a differential, reflection-type phase shifter," in *Proc. IEEE Int. Symp. Phased Array Syst. and Technol. (ARRAY)*, Oct. 2010, pp. 225–232.

[3] D. G. Kam, D. Liu, A. Natarajan, S. Reynolds, and B. Floyd, "Low-cost antenna-in-package solutions for 60-GHz phased-array systems," in *Proc. IEEE Conf. Electrical Performance of Electronic Packag. and Syst. (EPEPS)*, Oct. 2010, pp. 93–96.

[4] A. Natarajan, A. Komijani, X. Guan, A. Babakhani, and A. Hajimiri, "A 77-GHz phased-array transceiver with on-chip antennas in silicon: Transmitter and local LO-path phase shifting," *IEEE J. Solid-State Circuits*, vol. 41, no. 12, pp. 2807–2819, Dec. 2006.

[5] K. M. Nguyen, A. Accardi, G. W. Wornell, and C. G. Sodini, "Digital phase tightening for millimeter-wave imaging," presented at the IEEE Custom Integrated Circuits Conf. (CICC), San Jose, CA, USA, Sep. 2010.

[6] L. Khuon, E. W. Huang, C. G. Sodini, and G. W. Wornell, "Integrated transceiver arrays for multiple antenna systems," in *Proc. Vehic. Technol. Conf. (VTC)*, Stockholm, Sweden, May 2005.

[7] M. Elkhouly, C.-S. Choi, S. Glisic, C. Scheytt, and F. Ellinger, "Millimeter-wave beamforming circuits in SiGe BiCMOS," in *Proc. IEEE Bipolar/BiCMOS Circuits and Technol. Meet. (BCTM)*, Oct. 2010, pp. 129–132.

[8] Y. Sato, K. Fujita, H. Sawada, and S. Kato, "Design and performance of beam-forming antenna with discrete phase shifter for practical millimeter-wave communications systems," in *Proc. Asia-Pacific Microwave Conf. (APMC)*, Dec. 2010, pp. 638–641.
[9] D. Ehyaie and A. Mortazawi, "A new approach to design low cost, low complexity phased arrays," in *IEEE Int. Microwave Symp. (MTT-S) Dig.*, May 2010, pp. 1270–1273.
[10] S. Norsworthy, R. Schreier, and G. Temes, *Delta-Sigma Data Converters: Theory, Design, and Simulation*. New York, NY, USA: IEEE Press, 1996.
[11] B. Almutairi and M. Kraft, "Experimental study of single loop sigma-delta and multi-stage noise-shaping (MASH) modulators for MEMS accelerometer," in *Proc. IEEE Sensors*, Oct. 2011, pp. 520–523.
[12] W. Almeida, G. Freitas, L. Palma, S. Catunda, R. Freire, H. Aboushady, F. Santos, and A. Oliveira, "A constant temperature thermoresistive sigma-delta anemometer," presented at the Instrumentation Measurement Technol. Conf. (IMTC), May 2007.
[13] S. Thoss, O. Machul, and B. Hosticka, "A novel architecture for inductive proximity sensors using sigma delta modulation," in *Proc. Eur. Solid State Circuits Conf. (ESSCIRC)*, Sep. 2007, pp. 284–287.
[14] G. Altinok, M. Al-Janabi, and I. Kale, "Improved sigma-delta ultrasound beamformers with adaptive low-pass decimation filters," presented at the IEEE Instrumentation, Measurement Technol. Conf. (IMTC), May 2011.
[15] H. Bilge and M. Karaman, "Subarray delta-sigma beamforming for ultrasonic imaging," in *Proc. IEEE Ultrasonics Symp.*, Oct. 2002, vol. 2, pp. 1623–1626.
[16] P. Silva, V. Correia, S. M. Lanceros, and J. Rocha, "Sigma-delta A/D converter for CMOS image sensors," in *Proc. Int. Conf. Microelectron. (ICM)*, Dec. 2009, pp. 94–97.
[17] M. Kozak and M. Karaman, "Digital phased array beamforming using single-bit delta-sigma conversion with non-uniform oversampling," *IEEE Trans. Ultrason., Ferroelectr., Freq. Contr.*, vol. 48, no. 4, pp. 922–931, Jul. 2001.
[18] H. Aomori, T. Otake, N. Takahashi, I. Matsuda, S. Itoh, and M. Tanaka, "An oversampling 2D sigma-delta converter by cellular neural networks," in *Proc. IEEE Int. Symp. Circ., Syst. (ISCAS)*, Jun. 2010, pp. 2566–2569.
[19] T. Kite, B. Evans, A. Bovik, and T. Sculley, "Digital halftoning as 2-D delta-sigma modulation," in *Proc. Int. Conf. Image Process.*, Oct. 1997, vol. 1, pp. 799–802.
[20] D. Scholnik, J. Coleman, D. Bowling, and M. Neel, "Spatio-temporal delta-sigma modulation for shared wideband transmit arrays," in *Proc. IEEE Radar Conf.*, Apr. 2004, pp. 85–90.
[21] C.-P. Yeang, G. W. Wornell, L. Zheng, and J. Krieger, "Dense transmit and receive antenna arrays," presented at the IEEE Int. Symp. Antennas, Propagat. Soc. (APSURSI), 2010.
[22] C.-P. Yeang, G. W. Wornell, L. Zheng, and J. Krieger, "Dense transmit and receive phased arrays," in *Proc. IEEE Int. Symp. Phased Array Syst. and Technol. (ARRAY)*, 2010, pp. 934–939.
[23] J. Kong, *Electromagnetic Wave Theory*. New York, NY, USA: Higher Education Press, 2002.
[24] D. M. Pozar, *Microwave Engineering*. Hoboken, NJ, USA: Wiley, 2005.
[25] I. Gupta and A. Ksienski, "Effect of mutual coupling on the performance of adaptive arrays," *IEEE Trans. Antennas Propag.*, vol. 31, no. 5, pp. 785–791, 1983.
[26] J. de Mateo García and A. G. Armada, "Effects of bandpass sigma-delta modulation on OFDM signals," *IEEE Trans. Consumer Electron.*, vol. 45, no. 2, pp. 318–326, 1999.
[27] W. Wasylkiwskyj and W. Kahn, "Theory of mutual coupling among minimum-scattering antennas," *IEEE Trans. Antennas Propag.*, vol. 18, no. 2, pp. 204–216, 1970.
[28] R. C. Hansen, *Phased Array Antennas*. Hoboken, NJ, USA: Wiley Interscience, 2009.

**James D. Krieger** received the B.S. degree in physics from the University of California at Santa Barbara, Goleta, CA, USA, in 2000 and the M.S. degree in electrical engineering from the Ohio State University, Columbus, OH, USA, in 2005. He is currently pursuing the Ph.D. degree at the Massachusetts Institute of Technology, Cambridge, MA, USA.

From 2001 to 2003 and 2005 to 2008, he was a Researcher at MIT Lincoln Laboratory, Lexington, MA, USA, where his primary focus was the development and analysis of wideband antenna and array systems.

**Chen-Pang Yeang** (M'06) received the B.S. degree (1992) from National Taiwan University, Taipei, and the S.M. (1996) and Sc.D. degrees (1999) from the Massachusetts Institute of Technology (MIT), Cambridge, MT, USA, all in electrical engineering, and the Ph.D. degree (2004) in the history and social study of science and technology from MIT.

He was a Research Assistant (1994–99) and a Postdoctoral Associate (2000, 2001, 2005–06) at MIT Research Laboratory of Electronics, a Graduate Fellow (2002–04) and a Postdoctoral Fellow (2004–06) at the Dibner Institute for the History of Science and Technology, Cambridge, MA, USA, a Visitor at the Division of Humanities and Social Sciences at California Institute of Technology (2002), Max Planck Institute for the History of Science, Berlin (2006), and the Institute of Modern History, Academia Sinica, Taipei (2008). He is an Associate Professor at the Institute for the History and Philosophy of Science and Technology, University of Toronto, and a Member at the School of Historical Studies, Institute for Advanced Study, Princeton (2012–13). He is a historian and electrical engineer. His research areas have included the history of modern physical sciences and technology, electromagnetic theory, antennas, and synthetic aperture radar. He authored the book *Probing the Sky with Radio Waves* (University of Chicago Press, 2013) on the history of radio-wave propagation and is launching a research project on the history of noise in the first half of the twentieth century.

Dr. Yeang was selected as the 2004–2005 Life Member Fellow in Electrical History by the IEEE History Committee, and is a recipient of the Standard Research Grant from the Social Sciences and Humanities Research Council of Canada (2010–14). He is on the Advisory Board of the journal East Asian Science, Technology, and Society. He is also a Member of the IEEE, History of Science Society, and Society for the History of Technology.

**Gregory W. Wornell** (S'83–M'91–SM'00–F'04) received the B.A.Sc. degree in electrical engineering from the University of British Columbia, Vancouver, BC, Canada, and the S.M. and Ph.D. degrees in electrical engineering and computer science from the Massachusetts Institute of Technology, Cambridge, MA, USA, in 1985, 1987, and 1991, respectively.

Since 1991, he has been on the faculty at MIT, where he is the Sumitomo Professor of Engineering in the Department of Electrical Engineering and Computer Science (EECS) and leads the Signals, Information, and Algorithms Laboratory in the Research Laboratory of Electronics, and co-chairs the EECS Department Graduate Program. He has held visiting appointments at the former AT&T Bell Laboratories, Murray Hill, NJ, USA, the University of California, Berkeley, CA, USA, and Hewlett-Packard Laboratories, Palo Alto, CA. His research interests and publications span the areas of signal processing, digital communication, and information theory, and include algorithms and architectures for wireless networks, sensing and imaging systems, digitally-enhanced analog circuits and systems, multimedia applications, and aspects of computational biology and neuroscience.

Dr. Wornell has been involved in the Information Theory and Signal Processing Societies of the IEEE in a variety of capacities, and maintains a number of close industrial relationships and activities. He has won a number of awards for both his research and teaching.